CONTROLLING SYNCHRONISATION THROUGH ADAPTIVE PHASE LAGS

Markus Brede
Department of Electronics and Computer Science
University of Southampton
United Kingdom
markus.brede@soton.ac.uk

Alexander C. Kalloniatis
Joint and Operations Analysis Division
Defence Science and Technology Group
Australia
alexander.kalloniatis@dsto.defence.gov.au

Abstract

We compare two methods for controlling synchronisation in the Kuramoto model on an undirected network. The first is by driving selected oscillators at a desired frequency by linking to an external driver, and the second is by including adaptive lags within the Kuramoto interactions, where the lags evolve according to a dynamics involving the reference frequency. Performing numerical simulations, we find that driving via adaptive lags allows for stronger alignment to the external driver at lower cost. Numerical results are backed up by equilibrium analysis based on a fixed point ansatz assuming frequency synchronised clusters and solving the spectrum of the associated Jacobian. A simple intuitive model emerges based on the interaction between splayed clusters close to a critical point.

Key words

Synchronisation; networks; control; adaptive; external driver

1 Introduction

The ability of networks of coupled entities to achieve synchronised dynamics is fundamental to a variety of scientific applications, from physical, chemical, biological and even social systems. To this end, the Kuramoto model [Kuramoto, 1984] on a network, defined by

$$\dot{\theta}_i = \omega_i + \frac{K}{N}\sum_{j=1}^{N} A_{ij}\sin(\theta_j - \theta_i), \qquad (1)$$

combines a number of simple features yet exhibits rich behaviours (see [Acebron et al., 2005; Dorogovtsev, Goltsev and Mendes, 2008; Arenas, 2008; Doerfler and Bullo, 2014] for recent reviews). Here θ_i is a time-dependent phase angle at node i of a network of N nodes of a graph $\mathcal{G}$ given by the adjacency matrix A_{ij}, with ω_i the native frequencies drawn from some statistical distribution. The model is well known to display a critical transition for the complete graph for $N \to \infty$ at some coupling K at which a proportion of oscillators spontaneously synchronise to a frequency that is the mean of the native frequency ensemble $\bar{\omega}$; the normalised coupling may be absorbed into a constant $\sigma \equiv \frac{K}{N}$. At couplings beyond this the phase differences between them tend to zero. Many papers have explored this and the role of topology in influencing this effect [Hong, et al., 2002; Ichinomiya, 2004; Restrepo, Ott and Hunt, 2007; Oh et al., 2006; Gómez-Gardenes, Moreno and Arenas, 2007] or the inter-relationship between topology and the frequency allocation on the network [Brede, 2008]. More recently attention has turned to control problems in this context. The standard approach to control on a network is to attach external controllers to the nodes on which are defined a linear dynamical system, and pose the analogous question to the Kalman filter [Stengel, 1994]: is the network controllable in the sense of any final state being reachable from any initial state? In synchronisation problems this is more narrowly defined: can the system be controlled to reach synchrony from any random initial condition. Implicit in this objective is synchrony to the mean of the frequency ensemble. In this paper we shall explore a generalisation of this, to seek improved synchronisation, at lower 'cost' – in terms of coupling strength – and, significantly, to frequencies other than the mean of the ensemble of native frequencies.

The classical work on external controllability on networks is that of Liu, Slotine and Barabasi [Liu, Slotine and Barabasi, 2011] who adapt the Kalman filter approach. As inferred, here the objective is to guarantee that any final state of a vector of variables X_i is achievable from any initial input using linear control. More recently, the work has also been generalised to some forms of non-linear control by Arsiwalla, Barzel and Barabasi [Arsiwalla, 2016]. Within the linear model, problems of minimum number of nodes and minimum cost have been explored by Li et

al. [Li et al., 2016]. Within synchronisation problems, the final state is more prescribed, namely frequency- or phase-synchrony. Hamiltonian control for the Kuramoto model has been explored by Gjata et al [Gjata et al., 2016], where the Kuramoto model can be written in Hamilton form using action-angles variables [Garcia-Morales, Pellicer and Manzanares, 2008; Kalloniatis, 2014; Witthaut and Timme, 2014]. However this method works in the regime of partial synchronisation where perturbations then allow the fully synchronised state to be achieved. Closer in spirit to our approach, an adaptive model of control has been explored by Eom, Boccaletti and Caldarelli [Eom, Boccaletti and Caldarelli, 2016], but where the network itself evolves through a fitness model to improve synchronisation. An alternative approach considers an adaptive coupling [Skardal, Taylor and Restrepo, 2014]. In all of these cases the adaptation improves synchronisation to the mean frequency. Are different collective frequencies possible? May control facilitate this?

Our paper takes its cue from the lesser-known Kuramoto-Sakaguchi model which introduces a phase lag or frustration λ_i

$$\dot{\theta}_i = \omega_i + \frac{K}{N}\sum_{j=1}^{N} A_{ij}\sin(\theta_j - \theta_i + \lambda_i), \qquad (2)$$

This model is known for the property that the system does not synchronise to the mean of the ensemble by virtue of the absence now of the antisymmetry of the interaction function. In [Lohe, 2015], it was observed that such lags may be used to control the system to a predefined frequency for the complete network case. In our previous paper [Brede and Kalloniatis, 2016] we showed how a codynamics, where the λ_i become functions of time with their own evolution equation, can improve synchronisation – indeed, achieve perfect phase synchronisation. This arises essentially because the phase shifts achieve an equilibrium configuration that overcomes the barrier posed by the non-uniform native frequencies for perfect synchronisation $\theta_i = \theta_j$. In this paper we modify this adaptive lag mechanism to show how it can become a control model in the sense of guaranteeing synchronisation to a specified external frequency. However, an external control version of this is also possible – to which we compare the adaptive lag model. We find, in fact, that the adaptive model is more efficient in terms of required controlled nodes at achieving the desired frequency and with better synchronisation. In this paper we focus on relatively small networks of $N = 40$ where we can elucidate the underlying mechanisms, however we have run the full numerical computations for larger scale systems, for $N \sim 1000$.

The paper is structured as follows. First we outline the adaptive and reference models explicitly. We then show a range of numerical simulations of the model for a network of $N = 40$ nodes, and identify the different phases of the system. We then conduct a fixed point analysis to examine how stability properties relate to the regimes we observe numerically. Important for this will be an *ansatz* based on two clusters of nodes on the network – those subject to control and those not. We then probe particular regions of the phase diagram. We finally summarise and conclude.

2 Adaptive lags vs external control

We compare two models where Kuramoto sychronisation is controlled to some external driving frequency Ω. The first we may refer to as a reference model:

$$\dot{\theta} = \omega_i + \sigma\sum_j A_{ij}\sin(\theta_j - \theta_i) + \eta b_i \sin(\Omega t - \theta_i) \qquad (3)$$

Here, an oscillator θ_i couples to an external driver when $b_i = 1$ or is left to itself to synchronise according to its adjacent partners when $b_i = 0$. The driver strength is given by η.

An alternate model is one where *time-dependent* lags $\lambda_i(t)$ are introduced but which co-evolve with the θ_i:

$$\dot{\theta}_i = \omega_i + \sigma\sum_j A_{ij}\sin(\theta_j - \theta_i + \lambda_i)$$
$$\dot{\lambda}_i = \tau b_i \sin(\Omega t - \theta_i). \qquad (4)$$

Here again, when $b_i = 1$ the lags co-evolve and when $b_i = 0$ they are frozen in which case we assign initial condition $\lambda_i(0) = 0$, or simply $\lambda_i(0) = b_i\lambda$ with $\lambda \in (-\pi, \pi)$ drawn from a random uniform distribution. The phases θ_i corresponding to nodes with $b_i = 0$ then evolve according to their own local synchronisation interactions on the network. The constant τ here represents the time constant associated wth the dynamical lags. One motivation for the second model is our earlier work on adaptive lag dynamics $\dot{\lambda} = \tau\sum_j A_{ij}\sin(\theta_j - \theta_i)$ where we found this could enhance synchronisation compared to the ordinary Kuramoto dynamics while failing to guarantee the external collective frequency to which this synchronisation occurs. The present version elevates this interaction to a control model with explicit reference to an external driving frequency Ω.

We wish to compare the behaviours of these models in terms of driving phases to the external frequency, $\theta_i \approx \Omega t$, as functions of the various strengths η, τ as the density of control nodes, $\rho = \sum_i b_i/N$ varies between 0 and 1.

3 Numerical solutions

We begin by showing the results of numerical integration of the equations of motion for the two models. Using a fourth order Runge-Kutta method with step size

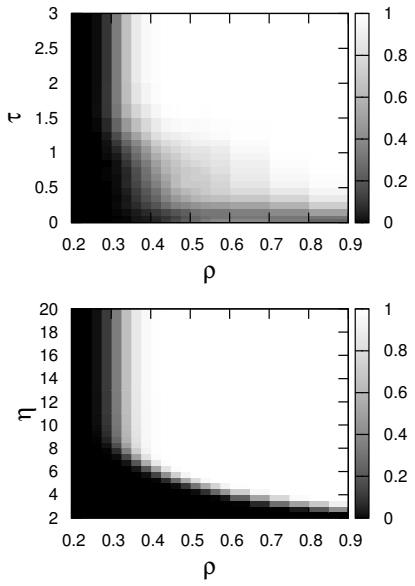

Figure 1. Phase diagram for random regular graph of $k = 8, N = 40$, showing the fraction of 100 instances achieving full synchronisation to the frequency Ω across the parameter space of ρ vs τ for the adaptive lag model (top) and ρ vs η for the externally driven reference model.

$\Delta t = 0.1$ we integrate out to $t = 5 \times 10^5$ time steps for $\sigma = 1$. Simulations are carried out for random regular networks of degree $k = 8$, a deliberate choice to reduce effects of network heterogeneity in this initial investigation. Native frequencies ω_i are randomly drawn from the uniform distribution $[-1, 1]$ so that for each instance the average frequency $\bar{\omega} \approx 0$. We choose $\Omega = 2.5$ – a controlling frequency clearly outside the interval for the native frequencies. We scan across the remaining two parameters for the two models: (ρ, τ) for the adaptive lags and (ρ, η) for the externally driven model. The degree of synchronisation is measured by Kuramoto's order parameter

$$r = \langle \frac{1}{N} | \sum_j e^{i\theta_j} | \rangle \tag{5}$$

where $r = 1$ represents full synchronisation. We also measure the closeness of the average instantaneous frequency to the external frequency Ω via

$$\Delta = \langle \frac{1}{N} \sum_i |\dot{\theta}_i - \Omega)| \rangle, \tag{6}$$

where brackets indicate averages over time (after discarding a transient).

Numerical experiments show that given configurations either achieve very good synchronisation to the external frequency ($\Delta < 10^{-4}$) or fail to synchronise. Accordingly, for given densities of controlled oscillators ρ and given parameters τ or η we measure the fraction of configurations that achieved synchronisation to the external frequency. In Fig. 1 we show density plots for the fraction of configurations achieving full synchronisation to the frequency Ω: white regions indicate that systems achieve full synchrony, while black indicates regions in which configurations fail to synchronise. We note that for low values of τ transients become very long – which we shall explain later – and so for $\tau < 0.5$ one must integrate up to very large times to establish whether an instance has synchronised. Hence numerical results in this region have to be seen as a lower bound for the number of synchronised configurations.

First we observe a minimum density of controlled oscillators ρ for synchronisation to occur, which is the same for both models, i.e. $\rho_c \approx 0.3$. More interestingly, we see that the adaptive lag model allows for synchronisation to the driving frequency even at very small values of τ, whereas the reference model clearly requires substantial coupling strength η. The contrast with the reference model is unambiguous: below $\eta = 1$ systems do not synchronise at any ρ, while in the lag-controlled model at least some synchronised configurations are observed for any choice of τ. Close to 100% synchronised configurations are achieved for much lower values of $\tau \geq 1$ for the lag-controlled case as compared to $\eta \geq 8$ in the reference model.

In the following we seek to understand these behaviours more analytically using fixed point analysis.

4 A two cluster *ansatz* for lag model

Prompted by the observation in the previous section that for general ρ synchronisation to the external frequency, though very high, is never quite perfect, we perform an equilibrium analysis allowing for two clusters in the fixed point *ansatz*: one consisting of the oscillators that phase synchronise alongside controlling phase lags ($b_i = 1$), identified by nodes in a sub-graph, which we denote $i \in \mathcal{G}_1$, and the other those nodes with without lags ($b_i = 0$), $i \in \mathcal{G}_2 = \mathcal{G} - \mathcal{G}_1$. So the *ansatz* reads

$$\begin{aligned} \theta_i(t) &= \Omega t + \vartheta_i(t), i \in \mathcal{G}_1 \\ \theta_i(t) &= \Omega t + \alpha_i + \varphi_i(t), i \in \mathcal{G}_2 \\ \lambda_i(t) &= \mu_i + \chi_i(t) \end{aligned} \tag{7}$$

with ϑ_i, φ_i and χ_i considered small fluctuations.

One of us has used *ansaetze* such as this in the study of a multi-network generalisation of the Kuramoto model [Kalloniatis and Zuparic, 2016; Holder, Zuparic and Kalloniatis, 2017], where we allow for two or three relatively shifted but internally phase synchronised clusters. Within such tight constraints, a great deal of analytical tractability is obtained. Here we relax the requirement of exact phase synchronisation within the

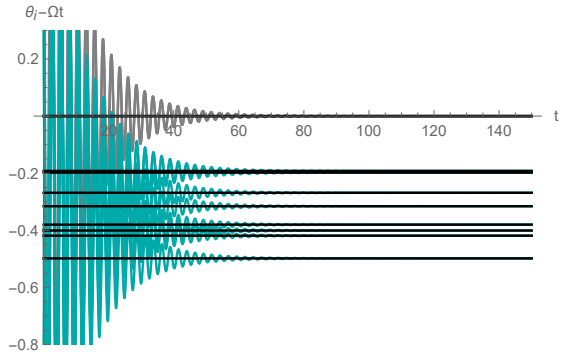

Figure 2. Example of clustering for $N = 40, \rho = 0.8$ where grey are the controlled $\theta_i - \Omega t$, cyan are the uncontrolled $\theta_i - \Omega t$ and black are the α_i derived from Eq. (11).

second cluster. In this respect we allow the cluster to display an arbitrary degree of 'splay', $\alpha_i \neq \alpha_j$, whose consequences will be seen below.

Expanding the equations of motion Eqs. (4) we obtain

$$\begin{aligned}
\dot{\vartheta}_i &= \omega_i - \Omega + \sigma k_i^{(1)} \sin\mu_i + \sigma k_i^{(2)} \sin(\alpha_i + \mu_i) \\
&\quad + \mathcal{O}_i^{(1)}(\vartheta, \varphi, \chi) \\
\dot{\varphi}_i &= \omega_i - \Omega - \sigma k_i^{(1)} \sin\alpha_i + \sigma \sum_{j \in \mathcal{G}_2} A_{ij} \sin(\alpha_j - \alpha_i) \\
&\quad + \mathcal{O}_i^{(2)}(\vartheta, \varphi, \chi) \\
\dot{\chi}_i &= -\tau \varphi_i
\end{aligned} \tag{8}$$

where $k_i^{(a)}$ is the degree of node i with respect to nodes in the sub-graph $\mathcal{G}_a$, and $\mathcal{O}_i^{(a)}$ are linear in the fluctuations. Note here that we may form the fluctuations into a super-vector $v = (\vartheta, \varphi, \chi)$ so that the overall linearised system takes the form

$$\dot{v} = W - \Lambda v, \tag{9}$$

with Λ the Jacobian which we give explicitly in the next section. Thus steady-state solutions, if the system is stable, are $v^* = \Lambda^{-1} W$ after removal of any zero-modes (or alternately, using the pseudo-inverse).

Requiring that the $\dot{v}$ vanish, so that all the constant parts are in the parameters μ_i, α_i, gives:

$$\omega_i - \Omega + \sigma k_i^{(1)} \sin\mu_i + \sigma k_i^{(2)} \sin(\alpha_i + \mu_i) = 0, \quad i \in \mathcal{G}_1, \tag{10}$$

$$\omega_i - \Omega - \sigma k_i^{(1)} \sin\alpha_i + \sigma \sum_{j \in \mathcal{G}_2} A_{ij} \sin(\alpha_j - \alpha_i) = 0, \quad i \in \mathcal{G}_2. \tag{11}$$

Eqs. (10,11) define now the fixed point manifold. The obvious procedure is to use the second of these, Eq. (11), which is μ_i independent, to solve for α_i first and then use these in the first Eq. (10) to solve for the μ_i. The α_i equation may be simplified by allowing for $\alpha_i - \alpha_j$ to be small allowing the $\sin(\alpha_j - \alpha_i)$ term to be re-expressed in terms of the graph Laplacian. Unfortunately, there is no analytical solution for this, so we do not pursue this option. However, the first equation may be solved for $\sin\mu_i$:

$$\begin{aligned}
\sin\mu_i = \Big(& -(\omega_i - \Omega)(k_i^{(1)} + k_i^{(2)} \cos\alpha_i) \\
& \pm k_i^{(2)} |\sin\alpha_i| [\sigma^2 (k_i^{(1)})^2 + 2 k_i^{(1)} k_i^{(2)} \cos\alpha_i \\
& + (k_i^{(2)})^2 - (\omega_i - \Omega)^2]^{\frac{1}{2}} \Big) / \\
& \Big(\sigma (k_i^{(1)})^2 + 2 k_i^{(1)} k_i^{(2)} \cos\alpha_i + (k_i^{(2)})^2 \Big) .
\end{aligned}$$

If we subject all nodes to control so that $\alpha_i = 0$, in which case $k_i = k_i^{(1)}$, then $\sin\mu_i = -\frac{\omega_i - \Omega}{\sigma k_i}$. Such a result for the equilibrium phase lags arises in [Brede and Kalloniatis, 2016] where a different model was used for the adaptive mechanism.

To illustrate clustering as one tight group and another splayed, we show in Fig. 2 a run of a random regular graph for $N = 40$ with $\rho = 0.8, \sigma = \tau = 1$. The plot shows the behaviour of $\theta_i - \Omega t$ for both controlled (gray) and uncontrolled (cyan) nodes. We see that the 32 controlled components, with $b_i = 1$, give $\theta_i = \Omega t$ demonstrating their perfect phase synchronisation. The remaining eight uncontrolled components show deviations from Ωt that are each slightly different from each other, and rapidly converge to the α_i as derived from Eq. (11), indicated in black.

5 Stability analysis of adaptive lags

In components, the Jacobian Λ^{AdLg} is:

$$\Lambda_{ij}^{\mathrm{AdLg}} = \begin{pmatrix} \Lambda_{ij}^{\vartheta\vartheta} & \Lambda_{ij}^{\vartheta\varphi} & \Lambda_{ij}^{\vartheta\chi} \\ \Lambda_{ij}^{\varphi\vartheta} & \Lambda_{ij}^{\varphi\varphi} & 0 \\ \tau\delta_{ij} & 0 & 0 \end{pmatrix}, \tag{12}$$

where

$$\begin{aligned}
\Lambda_{ij}^{\vartheta\vartheta} &= \sigma \cos\mu_i L_{ij}^{(11)} \\
&\quad + \sigma \sum_{j' \in \mathcal{G}_2} \cos(\alpha_{j'} + \mu_i) A_{ij'}^{(12)} \delta_{ij}, && (13) \\
\Lambda_{ij}^{\vartheta\varphi} &= -\sigma A_{ij}^{(12)} \cos(\alpha_j + \mu_i), && (14) \\
\Lambda_{ij}^{\vartheta\chi} &= -\sigma D_{ij}^{(11)} \cos\mu_i \\
&\quad - \sigma \sum_{j' \in \mathcal{G}_2} A_{ij'}^{(12)} \cos(\mu_i + \alpha_{j'}) \delta_{ij}, && (15) \\
\Lambda_{ij}^{\varphi\vartheta} &= -\sigma A_{ij}^{(21)} \cos\alpha_i, && (16) \\
\Lambda_{ij}^{\varphi\varphi} &= \sigma L_{ij}^{(22)} \cos(\alpha_i - \alpha_j) + \sigma D_{ij}^{(21)} \cos\alpha_i, && (17)
\end{aligned}$$

where $D_{ij}^{(ab)}$ represents the diagonal matrix of degrees of the nodes of sub-graph $\mathcal{G}_a$ connected to $\mathcal{G}_b$, and

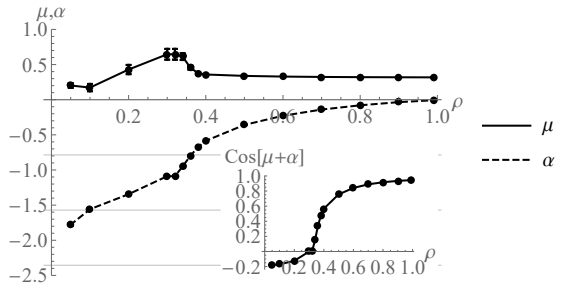

Figure 3. Plots of $\alpha = \frac{1}{N}\sum_i \alpha_i$ and $\mu = \frac{1}{N}\sum_i \mu_i$ from Eqs. (10,11) in the adaptive lag model for $N = 40$ random regular $k_i = 8$ with $\sigma = \tau = 1, \Omega = 2.5$, averaged over 300 instances, for different values of ρ. Note that these are independent of τ. Inset: plot of $\frac{1}{N}\sum_i \cos(\mu_i + \alpha_i)$ averaged over the same instances. Error bars here and in subsequent plots represent the standard error.

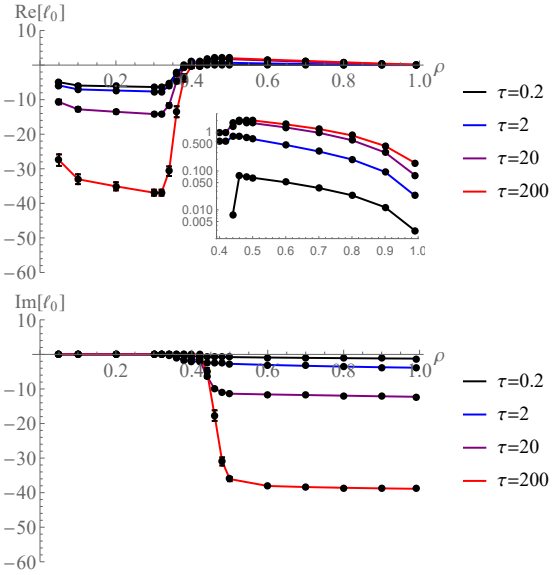

Figure 4. Top: plot of the average value of the real part of the lowest (in real part) eigenvalue of the super-Laplacian Λ^{AdLg} for $N = 40$ random regular $k_i = 8$ with $\sigma = 1, \Omega = 2.5$, averaged over 300 instances, as a function of the density of controlled nodes ρ and for different τ; inset the real part on logarithmic scale; bottom: plot of the imaginary part of the eigenvalue.

$L_{ij}^{(ab)} = D_{ij}^{(ab)} - A_{ij}^{(ab)}$ represents the corresponding Laplacian. The appearance of Laplacians of the various sub-graphs within these components means we will occasionally refer to Λ^{AdLg} as a 'super-Laplacian'.

The spectrum of the ordinary ('combinatorial') graph Laplacian [Bollobas, 1998] is generally known to play an important role in understanding coupled dynamical systems on networks [Pecora and Carroll, 1998]. While not quite as straightforward for the Kuramoto model, the lowest eigenvalue, known as the Fiedler [Fiedler, 1973], indicates the slowest transient of the system [Arenas, Diaz-Guilera and Pérez-Vincente, 2006] close to synchronisation. But the entire spectrum leaves an imprint in the dynamics across a range of coupling, even quite far from synchronisation [McGraw and Menzinger, 2008; Kalloniatis, 2010]. Much is known about the spectrum of the graph Laplacian for the classical graphs [Mohar, 1997], which enables us to infer some properties of the spectrum of Λ^{AdLg}.

In the absence of clustering, $\alpha_i = 0\ \forall\ i$, the super-Laplacian $\Lambda_{ij}^{\mathrm{AdLg}}$ involves factors of $\cos\mu_i$, a form quite close to that encountered in our previous work [Brede and Kalloniatis, 2016], and also not dissimilar from that found from a stability analysis of the ordinary Kuramoto-Sakaguchi model, Eq. (2). We know there that $\cos\mu_i > 0$ provides a necessary condition for stability. We thus can expect thresholds for instability when $\alpha_i \neq 0$. Moreover, Λ^{AdLg} here is not symmetric, so we expect a complex valued spectrum.

To proceed numerically now, we use Mathematica considering a random regular network again of degree $k_i = 8$ but consisting of $N = 40$ nodes. We set $\sigma = 1$ and choose $\Omega = 2.5$ as a case of an external frequency well outside the range of frequencies $\omega_i \in (-1, 1)$. We use values $\tau = 1, 10, 100$. To determine the spectrum of Λ^{AdLg} we compute α_i for $i \in \mathcal{G}_2$ from Eq. (11), followed by μ_i for $i \in \mathcal{G}_1$ from Eq. (10) and then with these the eigenvalues of Λ. The α_i, μ_i, which are evidently τ independent, are shown in Fig. 3. We observe that as ρ decreases the μ stay nearly constant while α increases in magnitude until $\rho = 0.4$, at which point even the equilibrium lag values increase up to $\rho = 0.3$.

We turn next to the lowest – in real part – eigenvalue which is, as anticipated above, complex valued. In Fig. 6 we plot this lowest eigenvalue, ℓ_0, as a function of the density of controlled nodes N_c, or alternatively of ρ, and for three choices of τ. Here we average over 300 frequency and graph instances for four values τ. Note that with our sign convention, a positive eigenvalue indicates *stability* of the fixed-point.

We observe a number of prominent features in Fig. 6: that for $\rho = 1$ the real part of the eigenvalue becomes extremely small while its imaginary part attains its largest value; and that below a certain threshold of $\rho = 0.3$ eigenvalues become negative real valued. The former result indicates long oscillatory transients in the dynamical approach to equilibrium while the latter result demonstrates instability of the dynamics. Indeed, we observe in full numerical solutions to the system at $\rho = 1$ long term oscillations while for small ρ the system seeks to synchronise to the mean frequency of the oscillator ensemble. Comparing these situations to full numerical solutions of the $N = 40$ case we observe oscillations for $\rho = 1$ even after $t = 10,000$, where corresponding results for $0.7 < \rho < 0.9$ show consistent convergence to equilibrium at the driving frequency $\Omega = 2.5$. Below $\rho = 0.7$ the transients to external synchronisation become longer and beyond the range of the Mathematica calculations used here. We also see, as predicted, that increasing τ has a more significant impact on the imaginary part of the lowest eigenvalue – in the stable regime. In the unstable regime, larger τ

has the effect of amplifying the negative real part. Note that the value of ρ at which the instability occurs does not change – because this only depends on the α_i, μ_j which are τ independant.

The origins of the instability may be understood by examining the values of α_i and μ_i across the range of ρ, as shown in Fig. 3. Note that as ρ decreases, the size of $\mathcal{G}_1$ decreases while that of $\mathcal{G}_2$ increases; thus the number of $\mu_i \neq 0$ decreases (fewer lags are introduced) and the number of $\alpha_i \neq 0$ increases. In Fig. 3 we highlight in both cases the position of the value of $-\pi/2$. It is evident that, for this size network, it is just below $\rho = 0.4$ that the sum $\alpha_i + \mu_j$ exceed $\pm\pi/2$ where the cosine factor in the super-Laplacian terms, such as $\Lambda^{\vartheta\vartheta}$, changes sign. From the inset of Fig. 3 we see that the averge value of $\cos(\mu_i + \alpha_i)$ indeed changes sign at $\rho = 0.3$. When $\rho = 0.3$ the μ_i achieve their largest average value – and this is where the instability is evident in the average eigenvalue. Because of this, the equilibria cease to be relevant below $\rho = 0.3$. At a more intuitive level, varying ρ means varying the population of tightly controlled oscillators in relation to the increasingly splayed uncontrolled oscillators. Instability is triggered once the splay of the latter population increases beyond a threshold where the combined phase lag and splay exceed $\pi/2$.

This final observation warrants a further comment. In previous experience with two-cluster approaches [Kalloniatis and Zuparic, 2016; Holder, Zuparic and Kalloniatis, 2017], we observed that the Lyapunov instability closely coincided with the point where the equations defining the equilibrium manifold, the analogues of Eqs. (10,11), failed to have static solutions. Thus, there, no instability on a static two-cluster solution was found. Here, even when increasing Ω we find that static solutions in many cases are obtainable – but the spectrum shows instability. This is simply a consequence of the fact that we now allow here an arbitrary degree of splay. The instability might be said to correspond to where the oscillators of sub-graph $\mathcal{G}_2$ might no longer be called a single 'cluster'.

In summary then, we see that the spectral properties in the vicinity of the two cluster fixed point explain both the long transients in dynamics for $\rho \to 1$, and increasing τ, as well as instability for lower values of ρ where the splay of only frequency synchronised uncontrolled nodes overwhelm the dynamics.

6 Stability analysis for reference model

We now perform a similar analysis for the reference control model. With the details given previously we may be a little circumspect here. Firstly, there are no explicit lags here, so in view of the *possibility* that perfect phase synchronisation *might* not be achievable we include μ_i in the *ansatz*

$$\begin{aligned}\theta_i(t) &= \Omega t + \mu_i + \vartheta_i(t), i \in \mathcal{G}_1\\ \theta_i(t) &= \Omega t + \alpha_i + \varphi_i(t), i \in \mathcal{G}_2.\end{aligned} \tag{18}$$

This gives for the fixed point (ignoring fluctuations after inserting the *ansatz* in the defining equations)

$$\begin{aligned}&\omega_i - \Omega + \sigma \sum_{j\in\mathcal{G}_1} A_{ij}\sin(\mu_j - \mu_i)\\ &+\sigma \sum_{j\in\mathcal{G}_2} A_{ij}\sin(\alpha_j - \mu_i) - \eta\sin\mu_i = 0,\\ &\qquad\qquad i \in \mathcal{G}_1,\end{aligned} \tag{19}$$

$$\begin{aligned}&\omega_i - \Omega + \sigma \sum_{j\in\mathcal{G}_1} A_{ij}\sin(\mu_j - \alpha_i)\\ &+\sigma \sum_{j\in\mathcal{G}_2} A_{ij}\sin(\alpha_j - \alpha_i) = 0,\\ &\qquad\qquad i \in \mathcal{G}_2.\end{aligned} \tag{20}$$

The Jacobian is now a two-by-two block form

$$\Lambda^{\rm Ref}_{ij} = \begin{pmatrix} \Lambda^{\vartheta\vartheta}_{ij} & \Lambda^{\vartheta\varphi}_{ij} \\ \Lambda^{\varphi\vartheta}_{ij} & \Lambda^{\varphi\varphi}_{ij}\end{pmatrix}, \tag{21}$$

where the individual entries are:

$$\begin{aligned}\Lambda^{\vartheta\vartheta}_{ij} &= \sigma L^{(11)}_{ij}\cos(\mu_i - \mu_j)\\ &\quad +\sigma \sum_{j'\in\mathcal{G}_2} A^{(12)}_{ij'}\cos(\alpha_{j'} - \mu_i)\delta_{ij}\\ &\quad +\eta\cos\mu_i,\end{aligned} \tag{22}$$

$$\Lambda^{\vartheta\varphi}_{ij} = -\sigma A^{(12)}_{ij}\cos(\alpha_j - \mu_i), \tag{23}$$

$$\Lambda^{\varphi\vartheta}_{ij} = -\sigma A^{(21)}_{ij}\cos(\mu_j - \alpha_i), \tag{24}$$

$$\begin{aligned}\Lambda^{\varphi\varphi}_{ij} &= \sigma L^{(22)}_{ij}\cos(\alpha_i - \alpha_j)\\ &\quad +\sigma \sum_{j'\in\mathcal{G}_1} A^{(21)}_{ij'}\cos(\mu_{j'} - \alpha_i)\delta_{ij}.\end{aligned} \tag{25}$$

These entries are more standard weighted Laplacians, apart from the shift $\eta\cos\mu_i$ whose sign is contingent on the μ_i. Overall $\Lambda^{\rm Ref}$ is symmetric, and therefore we may expect a purely real spectrum but with a shift in the lowest eigenvalue according to the values of μ_i. Alternately put, for $\eta = 0$, $\Lambda^{\rm Ref}$ has zero row and column sums and therefore has a spectrum bounded below by a zero eigenvalue.

We compute first the equilibrium values of α_i and μ_i from Eqs. (19,20) which are shown in Fig. 5. Note that these are now μ-dependent so the figure is somewhat more complex. At one extreme, $\eta = 100$, the α_i depend on ρ inversely to the induced lags μ_i for the controlled oscillators. Evidently, with such strong driving the controlled oscillators achieve very small phase lags. As ρ is reduced, the number of uncontrolled oscillators increases so that a splay develops in this group, with α_i increasing in magnitude. As η decreases the cross-over becomes marked. Importantly, very high coupling η to the driving frequency is required to achieve 'perfect phase synchronisation' $\mu_i \approx 0$. At the other extreme,

$\eta = 1$, the driving is so weak that the underlying Kuramoto interaction, with coupling σ, causes even the driven oscillators to be splayed. As ρ decreases, fewer oscillators are driven, so more may participate in the Kuramoto interaction. To say more beyond the crossover point requires completing the stability analysis.

We show the lowest eigenvalue as a function of ρ for different η in Fig. 6. We observe a clear transition as ρ decreases, the eigenvalue correspondingly decreases until it reaches effectively zero. For $\eta = 1$ the eigenvalue is extremely close to zero.

To understand these behaviours we note that in the absence of the shift $\eta \cos \mu_i$ in $\Lambda^{\rm Ref}$, the lowest eigenvalue will always vanish. Thus, while the μ_i are small at large ρ (as in Fig. 5) the shift in the spectrum is positive. Once one of the μ_i cross the threshold of $-\pi/2$ the shift is negative. For $\eta = 1$, the μ_i are already large at $\rho = 1$ however at this point the combination

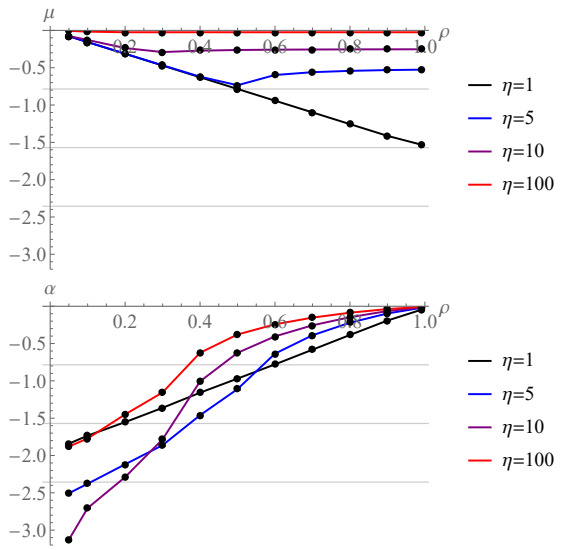

Figure 5. Plots of $\mu = \frac{1}{N}\sum_i \mu_i$ (left) and $\alpha = \frac{1}{N}\sum_i \alpha_i$ (right) in the externally driven model from Eqs. (20, 19) for $N = 40$ random regular $k_i = 8$ with $\sigma = \tau = 1, \Omega = 2.5$, averaged over 300 instances, as a function of ρ for different values of η.

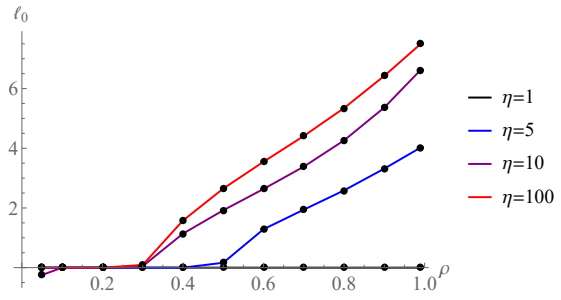

Figure 6. Plot of the average value of the lowest eigenvalue of the super-Laplacian $\Lambda^{\rm Ref}$ for $N = 40$ random regular $k_i = 8$ with $\sigma = 1, \Omega = 2.5$ as a function of the density of controlled nodes ρ and for different η.

$\eta \cos \mu_i$ is now less than one. As ρ decreases, the number of oscillators resisting the Kuramoto interaction decreases and so the natural Kuramoto dynamics allow some degree of convergence in phases – and hence the μ_i decrease. Intuitively, at $\eta = 1$, which equals the Kuramoto coupling $\sigma = 1$ chosen here, the externally driven is a larger frustrated Kuramoto system with a wider frequency distribution. For $\eta < 1$, not shown here, the shift $\eta \cos \mu_i$ in the spectrum assumes small non-zero values that fluctuate in sign around zero.

We conclude then that for $\eta > 1$ there is a transition to marginal stability for $\rho \approx 0.3$. Indeed we even see that this threshold value in ρ varies with η in the range $1 < \eta < 5$, a property seen in the numerical results of Fig. 1. In contrast to the adaptive lag model, the transition here is not to an instability but to marginal stability which would require a higher order analysis to establish definitively the Lyapunov properties here.

7 Order parameter

We now compare for the two models numerical solution, Fig.7 (on a scale to make error bars discernible), to truncation to leading order around the equilibria of the order parameter r (inset). Using trigonometric formulae we have for the adaptive lag model

$$r^2 \approx 1 - \frac{2}{N^2}\left(2N_c \sum_{i\in\mathcal{G}_2} \sin^2(\alpha_i/2) + \sum_{i,j\in\mathcal{G}_2} \sin^2((\alpha_i - \alpha_j)/2)\right) \qquad (26)$$

and for the externally driven model

$$r^2 \approx 1 - \frac{2}{N^2}\left(\sum_{i,j\in\mathcal{G}_1} \sin^2((\mu_i - \mu_j)/2) + 2\sum_{i\in\mathcal{G}_1, j\in\mathcal{G}_2} \sin^2((\mu_i - \alpha_j)/2) + \sum_{i,j\in\mathcal{G}_2} \sin^2((\alpha_i - \alpha_j)/2)\right). \qquad (27)$$

We use the equilibrium (μ_i, α_i) to compute r here and only include results down to the ρ value where the *ansatz* becomes unstable.

Both numerical and analytical approaches show high synchronisation down to densities of $\rho = 0.3$. The discrepancy between the two may be attributed to transients persisting in the numerical results and to the need for higher order corrections in the fluctuation expansion in the reference model when marginal stability arises. We have computed analogous numerical results for $\eta = 3$ and see that no stable configurations appear below $\rho = 0.75$. Thus there is consistency between

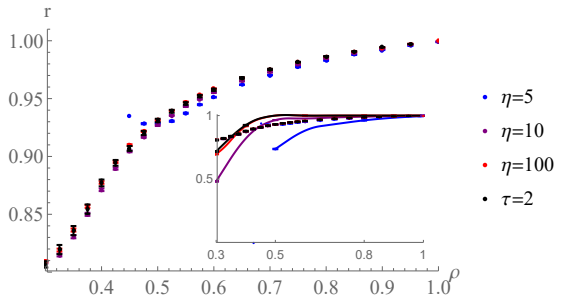

Figure 7. Plot of the order parameter r from numerical calculation for $\eta = 5, 10, 100$ in the externally driven model and $\tau = 2$ for the adaptive lag model; inset, combining numerical and approximate results based on Eqs. (26,27).

analytical and numerical results in that higher η is required to enable the externally driven model to reach the same levels of synchronisation down to the same densities of controllers as the adaptive lag model.

8 Conclusion

We compared two models for controlling synchronisation of Kuramoto oscillators to a desired external frequency different from the mean of the native frequencies. Even though both models exhibit similar transition points in the density of controllers, the adaptive lags model is better than driving a proportion of the oscillators externally: it achieves high levels of synchronisation for couplings that can be an order of magnitude weaker than the corresponding coupling to external drivers. Essentially, the lag model enables nearly exact phase synchronisation for the driven population – because of the dynamical adaptive mechanism – while the externally driven version never truly achieves phase synchronisation for even the driven subset.

The mechanism for this achievement of perfect synchronisation can be understood in terms of stability properties at the fixed point and intuitively in terms of the splaying effects within the driven and non-driven oscillator populations. Remarkably, standard equilibrium analysis goes far in understanding the non-linear behaviours of these models – precisely because the target state in the control model corresponds to a regime where linearisation is effective.

Though we have reported here the results for $N = 40$, we have examined significantly larger graphs, which will be reported elsewhere. Extensions of this work will examine changes of topology – for example varying connectivities or exploring other classes of complex networks. We conclude that well-known methods from physics provide insight into control problems for dynamical systems on networks.

Acknowledgements

One of us (ACK) is supported through a Chief Defence Scientist Fellowship and expresses gratitude for the hospitality of the University of Southampton.

References

Acebron, J.A. et al. (2005). Rev.Mod.Phys. 77, 137.

Arenas, A., et al. (2008). Phys.Rep. 469, 93.

Arenas, A., Diaz-Guilera, A., Pérez-Vincente, C.J. (2006). Phys.Rev.Lett. 96,114102.

Arsiwalla, X.D. (2016). Conference on Complex Systems, Amsterdam, 2016

Bollobás, B., Modern Graph Theory, Graduate Texts in Mathematics, Springer, New York.

Brede, M. (2008). Eur.Phys.J.B 62, 87.

Brede, M., Kalloniatis, A.C. (2016). Phys.Rev.E 93, 062315.

Dörfler, F. Bullo, F. (2014). Automatica 50, 1539

Dorogovtsev, S.N., Goltsev, A.V. and Mendes, J.F.F. (2008). Rev.Mod.Phys. 80, 1275.

Eom, Y.-H., Boccaletti, S., Caldarelli, G. (2016) Scientific Reports 6, 27111, 2016/doi:10.1038.

Fiedler, M. (1973). Czech. Math. J. 23 (98), 298.

Gjata, O., et al. (2016). arXiv:1610.01640.

Garcia-Morales, V., Pellicer, J., Manzanares, J.A., (2008). Ann.Phys. 323, 1844-1858.

Gómez-Gardenes, J. Moreno, Y. Arenas, A. (2007). Phys.Rev. E 75, 066106.

Holder, A.B., Zuparic, M.L., Kalloniatis, A.C. (2017). Physica D 341, 10-32.

Hong, H., Choi, M.Y., Kim B.J. (2002). Phys.Rev. E 65, 026139.

Ichinomiya, T. (2004). Phys.Rev. E 70, 026116.

Kalloniatis, A.C. (2010). Phys.Rev.E 82, 066202.

Kalloniatis, A.C. (2014). Ann.Phys. 348, 127-143.

Kalloniatis, A.C., Zuparic, M.L. (2016). Physica A 447, 21-35.

Kuramoto, Y. (1984). Chemical Oscillations, Waves and Turbulence, Springer, Berlin.

Liu, Y., Slotine, J., Barabasi, A. (2011). Nature 473, 167.

Li, G., Hu, W., Xiao, G., Deng, L., Tang, P., Pei, J., Shi,L. (2016). New J. Phys. 18, 013012.

Lohe, M.A. (2015). Automatica 54, 114-123.

McGraw, P.N., Menzinger, M. (2008). Phys.Rev.E 77, 031102.

Mohar, B. (1997). Graph Symmetry: Algebraic Methods and Applications, Eds. G. Hahn, G. Sabidussi, NATO ASI Ser. C 497, Kluwer, 225-275.

Oh, E., Lee, D.-S., Kahng, B., Kim, D. (2007). Phys.Rev. E, 011104.

Pecora, L.M., Carroll, T.L. (1998). Phys. Rev. Lett. 80, 2109.

Restrepo, J.G., Ott, E., Hunt, B.R. (2007). Phys.Rev. E 75, 066106, 2007

Skardal, P.S., Taylor, D., Restrepo, J.G. (2014). Physica D 267, 27-35.

Stengel, R.F. (1994). Optimal control and estimation, Dover, USA.

Witthaut, D., Timme, M. (2014). Phys.Rev.E 90, 032917.